Asian Journal of Chemistry; Vol. 38, No. 9 (2026), 2501-2509
ASIAN JOURNAL OF CHEMISTRY
https://doi.org/10.14233/ajchem.2026.36287

Computational Design of Carbazole-Based D-π-A Sensitizers for High-Performance Dye-Sensitized Solar Cells

KAMAKSHI SHARMA, OMNA SINGH, NANDINI SINGH, MRIDULA GUIN*, and N.B. SINGH*

Department of Chemistry and Biochemistry, Sharda University, Greater Noida-201310, India

*Corresponding authors: E-mail: n.b.singh@sharda.ac.in; mridula.guin@sharda.ac.in

Received: 25 April 2026 *Accepted*: 27 August 2026 *Published online*: 5 September 2026 AJC-22479

Dye-sensitized solar cells (DSSCs) are considered as third-generation photovoltaic technology due to single-device architecture, simple fabrication and good performance. Metal-free organic dyes having a donor-π-acceptor (D-π-A) architecture, have attracted major attention of researchers due to the facts that their electrochemical and optical properties can easily be tuned. In this work, two carbazole-based organic dyes, M1 and M2, were computationally designed and tested as potential DSSC sensitizers using density functional theory (DFT) and time-dependent DFT (TD-DFT) methodology. Ground-state geometry optimization at the B3LYP/6-31G(d,p) level which revealed that M1 possesses a more planar molecular structure compared to M2, thereby facilitating enhanced π-conjugation and intramolecular charge transfer. Frontier molecular orbital analysis in both gas and solvent phases revealed that M1 exhibits slightly greater electronic delocalization and excitability compared to M2. Simulated UV-Vis absorption spectra showed strong visible-light absorption, with M1 displaying a red-shifted maximum absorption wavelength (λ_{max}) at 458.81 nm and good light-harvesting capability. Further studies of molecular electrostatic potential (MEP), natural bond orbital (NBO), density of states (DOS), partial density of states (PDOS), reorganization energy and photovoltaic parameters confirmed the favourable charge-transfer characteristics of M1 and M2. Although M2 has lower reorganization energy than M1, the other calculated properties favour M1, which exhibits more favourable optical and electronic characteristics and may be a promising candidate for further experimental evaluation.

Keywords: Carbazole, DFT, TD-DFT, Dye-sensitized solar cell, Frontier molecular orbitals, Intramolecular charge transfer.

INTRODUCTION

Dye-sensitized solar cells (DSSCs) are the third-generation photovoltaic devices that have attracted attention due to their low fabrication cost, colour tunability, mechanical flexibility and good performance under diffuse and indoor light. A DSSC consists of a sensitizer, semiconductor, electrolyte and counter electrode, with the sensitizer playing a key role in light absorption, dye regeneration and electron injection [1,2]. Among metal-free organic dyes, donor-π-acceptor (D-π-A) systems are widely studied due to their structural flexibility and tunable optical and electronic properties.

Carbazole is a useful donor unit for DSSC dyes owing to its electron-rich nature, thermal and chemical stability, good hole-transport properties and several positions available for structural modification. It can act as a donor as well as a π-conjugated unit in organic sensitizers [3,4]. Carbazole-based dyes have been reported in D-A, D-π-A, D-D-π-A and D-A-π-A configurations with different π-spacers and acceptor groups. Changes in the donor, π-spacer, conjugation length and anchoring group can affect the HOMO–LUMO energy gap, absorption wavelength, charge distribution, electron injection and charge recombination [3,4]. Such structural changes can be used to modify the visible-light absorption and intramolecular charge-transfer characteristics of the dyes [5,6].

The π-spacer provides a conjugated pathway between the donor and acceptor and has a direct effect on the electronic structure of the dye. Benzoxadiazole and benzothiadiazole are useful π-spacers for this purpose. Although their structures are similar, the oxygen and sulphur atoms differ in polarizability and electronegativity, which can alter conjugation, charge distribution and electron-transfer properties. Arunkumar & Anbarasan [7] studied DSSC sensitizers containing furan, 3,4-ethylenedioxythiophene, benzothiadiazole, quinoxaline and benzoxadiazole linkers and reported favourable optical and photovoltaic properties for the benzothiadiazole- and

benzoxadiazole containing dyes [7]. These findings provide a basis for comparing the effects of benzoxadiazole and benzothiadiazole within a common carbazole-based dye structure.

Computational methods such as density functional theory (DFT) and time-dependent density functional theory (TD-DFT) are useful for examining the structural and electronic properties of DSSC dyes. DFT calculations provide information on optimized molecular geometry, frontier molecular orbitals, energy levels and charge distribution, while TD-DFT can be used to study electronic transitions and absorption spectra [8,9]. Reorganization energies can further provide information related to the charge-transfer characteristics of the sensitizers. In present work, two carbazole-based sensitizers were designed by changing the π-spacer between benzoxadiazole and benzothiadiazole (Fig. 1). Carbazole was used as the donor unit, while cyanoacrylic acid was selected as the acceptor and anchoring group for TiO_2. The two dyes contain the same donor and acceptor units, with only the π-linker being varied. This design allows the effect of oxygen- and sulphur-containing linkers on the properties of the sensitizers to be examined under comparable structural conditions.

The designed dyes were studied using DFT and TD-DFT calculations. Their optimized geometries, frontier molecular orbitals, HOMO-LUMO energy gaps, UV-Vis absorption properties, charge-transfer characteristics and reorganization energies were evaluated. The results provide a comparison of the two π-linkers and their effects on the geometric, electronic and optical properties of the carbazole-based sensitizers, with the aim of identifying the more suitable structure for DSSC applications.

COMPUTATIONAL METHODOLOGY

The structural, optical and electronic properties of the designed dyes (M1 and M2) were investigated using density functional theory (DFT) and time-dependent DFT (TD-DFT) calculations. Molecular structures were constructed using GaussView 6.0 and optimized in the gas and solvent phases to obtain the ground-state geometries. No symmetry constraints were applied during geometry optimization. The ground state structures were optimized using the B3LYP/6-31G(d,p) level of theory [10-12] with the Gaussian 16 program [13]. This level of theory has been widely used for geometry optimization and the study of carbazole-based organic dyes [14-22]. The same level was adopted in the present work to allow comparison with related carbazole-based sensitizers. The UV-Vis absorption properties were calculated using the TD-DFT method with the CAM-B3LYP functional. CAM-B3LYP incorporates long-range correction into the B3LYP functional and is suitable for studying electronic excitations and charge-transfer transitions in donor-π-acceptor systems [23]. The calculated excitation energies and absorption spectra were used to examine the optical properties of the designed DSSC dyes.

Solvent effects are important in sensitizer design, as solvent polarity can influence molecular geometry, frontier orbital energies, intramolecular charge transfer (ICT) and absorption characteristics, which are relevant to dye-semiconductor energy alignment and DSSC performance [24]. Dichloromethane (DCM) was selected to represent the experimental solvent environment. Solvation effects were included using the conductor-like polarizable continuum model (CPCM), with DCM as the solvent medium [25,26].

Structural parameters, such as bond lengths and torsion angles, were examined in relation to molecular planarity, conjugation and charge-transfer characteristics. Electronic properties were calculated in both gas and DCM phases. The HOMO and LUMO energies, energy gap, ionization potential, electron affinity, chemical potential, electronegativity, hardness, softness and electrophilicity index were determined for both dyes. The excited-state and absorption properties of the dyes were investigated using TD-DFT calculations on the optimized ground-state geometries in DCM. Solvation effects were considered using the CPCM model with DCM as the solvent. The maximum absorption wavelength, oscillator strength, excitation energy and major orbital transitions were calculated for the low-lying singlet excited states. Frontier molecular orbital maps were examined to determine the spatial distribution of electron density and the direction of charge transfer upon excitation.

The electronic analysis included natural bond orbital (NBO) charge analysis, transition density matrix (TDM) analysis, partial density of states (PDOS) and molecular electrostatic potential (MEP) mapping. Electron and hole reorganization energies were calculated to assess structural relaxation associated with charge redistribution. These parameters were used to compare the two carbazole-based dyes and assess their suitability as DSSC sensitizers. All quantum-chemical calculations were performed using Gaussian 16, while wavefunction analyses were carried out with Multiwfn [27].

RESULTS AND DISCUSSION

Ground-state geometries: The optimized geometries of two carbazole dyes (M1 and M2) have been analyzed in both

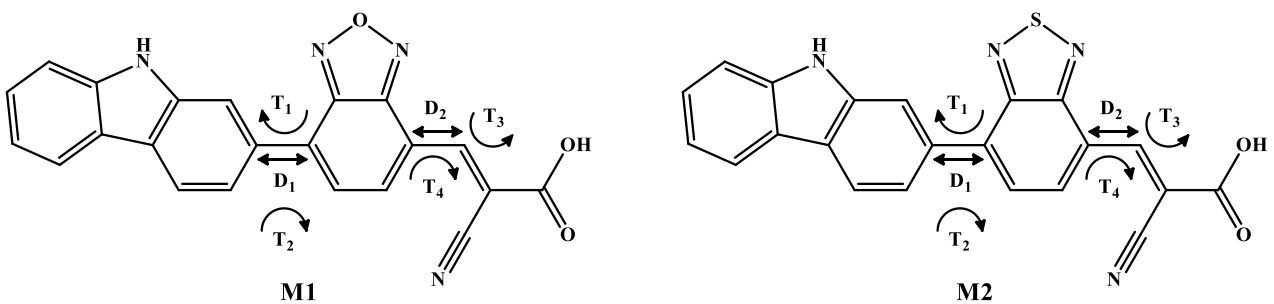

Fig. 1. Chemical structure of carbazole based dye molecules (M1 and M2)

TABLE-1
OPTIMIZED BOND DISTANCES AND TORSION ANGLES OF THE TWO DESIGNED CARBAZOLE DYES CALCULATED AT THE DFT/B3LYP/6-31G(d) LEVEL IN GAS AND SOLVENT PHASES

	Molecules	D1 (Å)	D2 (Å)	T1 (º)	T2 (º)	T3 (º)	T4 (º)
Gas phase	M1	1.47	1.44	26.98	26.33	179.64	0.54
	M2	1.44	1.47	34.07	32.51	179.36	0.80
Solution phase	M1	1.47	1.44	30.31	29.20	177.81	2.38
	M2	1.47	1.44	36.19	34.49	177.85	2.33

gas and solvent phases to assess their features relevant to their activity in the dye-sensitized solar cells (DSSCs) application. The most critical geometric parameters such as selected bond lengths and torsion angles were investigated since the planarity and conformational rigidity of the molecules significantly affect the inter and intra-conjugation charge transfer of the D-π-A sensitizers. The optimized structures of M1 and M2 in the gas phase is displayed in Fig. 2 and selected bond lengths and torsion angles are shown in Table-1. The bond length D1 and D2 in the gas phase are 1.47 Å and 1.44 Å for M1 and 1.44 Å and 1.47 Å for M2, respectively, revealing partial double bond character due to electron delocalization along the conjugated backbone [28,29]. This is better illustrated for the torsion angle values. It is found that M1 has lower values of T1 and T2 of 26.98º and 26.33º, respectively compared to M2 with values of T1 and T2 of 34.07º and 32.51º, respectively, implying that the M1 conformation is relatively more planar and can make a better orbital overlap between donor-bridge-acceptor skeleton. The bond distance in both structures remains very similar in the solvent phase, while the torsional angle values increase slightly *e.g.* 30.31º/29.20º for M1 and 36.19º/34.49º for M2, which means that both structures have a slight decrease in coplanarity after solvation. These changes in geometry are often observed in the absorption and efficiency of ICT in carbazole derivatives [30,31]. The geometric parameters suggest that M1 is more favourable for extended π-delocalization than M2. Its lower torsional distortion may facilitate stronger electronic communication between the donor and acceptor units, favouring more efficient intramolecular charge transfer [32,33].

Frontier molecular orbital (FMO) analysis: In DSSCs, the frontier molecular orbitals are accountable for light absorption, electron injection and dye regeneration. The gas-phase FMO energies show that M1 has HOMO and LUMO values of -6.254 and -3.695 eV, whereas M2 exhibits -6.128 and -3.519 eV, respectively. The HOMO-LUMO gaps are 2.559 eV and 2.608 eV for M1 and M2, respectively, which shows that M1 has a slightly smaller band gap compared to M2.

In the solvent phase, the HOMO and LUMO energies shift to -6.056 and -3.645 eV for M1 and to -5.991 and -3.475 eV for M2, reducing the energy gaps to 2.412 and 2.516 eV, respectively. The decrease in the difference in the solution phase indicates that the electronic states have become stabilized and that the tendency to excitation slightly decreased for both dyes. Some important quantum chemical descriptors computed for both gas and solution phase are listed in Table-2. The higher softness values calculated for M1 in both phases are consistent with its higher polarizability and capacity for charge redistribution.

TABLE-2
FRONTIER MOLECULAR ORBITAL ENERGIES AND GLOBAL REACTIVITY DESCRIPTORS OF THE DESIGNED CARBAZOLE DYES IN THE GAS PHASE AND SOLUTION PHASE

Parameters	Gas phase		Solution phase	
	M1	M2	M1	M2
HOMO (eV)	-6.255	-6.128	-6.056	-5.991
LUMO (eV)	-3.695	-3.519	-3.644	-3.474
ΔE = (LUMO-HOMO) (eV)	2.559	2.608	2.412	2.516
I = -E(HOMO) (eV)	6.255	6.128	6.056	5.991
A = -E(LUMO) (eV)	3.695	3.519	3.644	3.474
$\chi = (I + A)/2$ (eV)	4.975	4.368	4.849	4.733
$\mu = -\chi$ (eV)	-4.975	-4.368	-4.849	-4.733
$\eta = (I - A)/2$ (eV)	1.279	1.304	1.206	1.258
$S = 1/2\eta$ (eV)	0.391	0.383	0.415	0.397
$\omega = \mu^2/2\eta$ (eV)	9.669	7.315	9.751	8.901

The FMO energies of both dyes show favourable alignment for DSSC operation. The carbazole donor maintains the HOMO electron density, while the LUMO is mainly localized on the acceptor moiety, supporting intramolecular charge transfer. The 2D HOMO and LUMO surface maps and HOMO-LUMO energy gaps of M1 and M2 are shown in Fig. 3. The HOMO levels of both dyes lie below the redox potential of

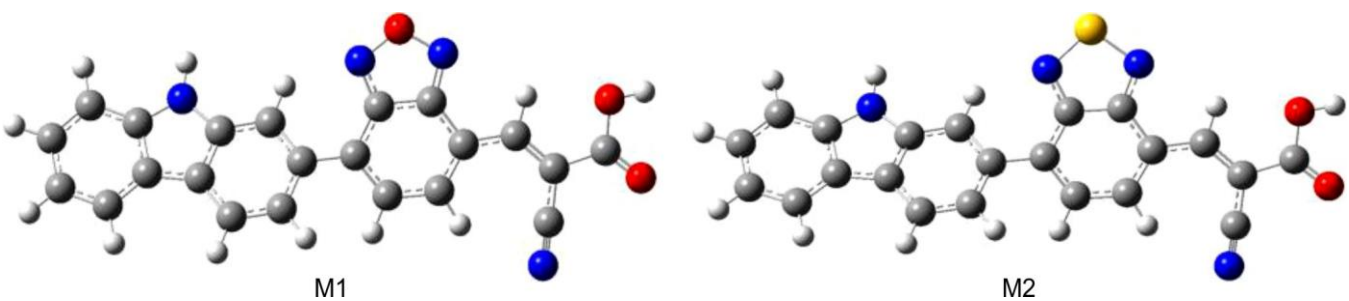

Fig. 2. DFT optimized structure of the dyes M1 and M2 in the gas phase

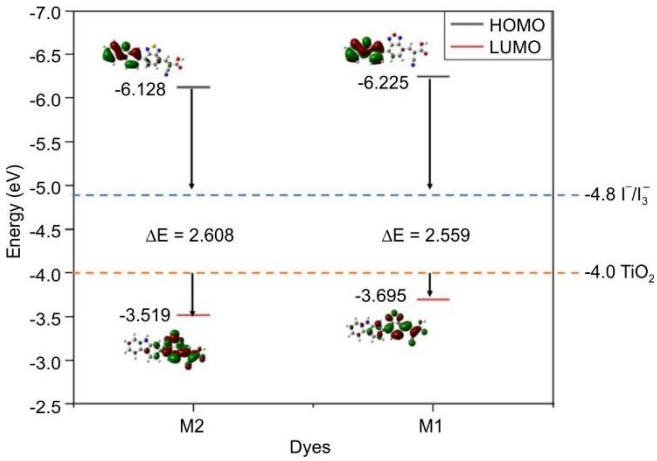

Fig. 3. FMO energy level diagram of the designed carbazole dyes showing HOMO and LUMO gap in relation to electronic excitation behaviour

the I^-/I_3^- electrolyte (-4.8 eV), providing a suitable energetic driving force for regeneration of the oxidized dyes. The LUMO levels are positioned above the conduction-band edge (CBE) of TiO_2 (-4.0 eV), allowing energetically favourable electron injection from the excited dyes into the semiconductor. M1 has a smaller HOMO-LUMO gap than M2, which may favour stronger visible-light absorption and charge transfer characteristics. The deeper HOMO levels of both dyes are favourable for dye regeneration [2].

UV-Vis absorption properties: The absorption spectral properties calculated from the TD-DFT simulation shows that both dyes are strong absorber of visible light. The absorption spectral properties of the two dye molecules are listed in Table-3 and simulated UV-Vis absorption spectra is depicted in Fig. 4. The dominant electronic transition being of low energy with λ_{max} at 458.81 nm for M1 and 441.95 nm for M2. The other two less intense absorptions of M1 are at 402.55 nm and 319.61 nm and for M2, the two minor absorptions are at 386.01 nm and 318.86 nm. The red-shifted and stronger S_0-S_1 transition for M1 is also in line with its lower HOMO-LUMO gap and better geometric planarity. Both dyes have the predominant transition to first excited state which is HOMO → LUMO in origin, with some contribution from HOMO-1 and HOMO-2 → LUMO transitions. This further validates the band gap characteristics of absorbing nature of the intramolecular charge-transfer transitions, which is a desirable and common property of carbazole based D-π-A sensitizers [34,35]. In both molecules, additional higher-energy transitions are found, but with lower oscillator strength and less light harvesting efficiency. The slightly higher oscillator strength and light-harvesting efficiency (LHE) of M1 suggest better photon absorption than M2. This agrees with previous reports that greater molecular planarity and a smaller band gap can favour broader or red-shifted absorption and improved sensitization properties [3,28].

NBO charge distribution and MEP analysis: Understanding of charge partitioning between the donor(carbazole), π-linker (benzoxadizole for M1 and benzothiodiazole for M2) and acceptor fragments (cyanoacrylic acid) of the two dyes in their ground state was achieved by natural bond orbital

TABLE-3
CALCULATED ABSORPTION SPECTRAL PROPERTIES OF THE TWO DESIGNED CARBAZOLE DYES OBTAINED FROM TD-DFT CALCULATIONS

Molecules	Electronic transitions	λ_{max} (nm)	E_{exc} (eV)	f_0	Transition	C.I. (%)	LHE
M1	$S_0 \rightarrow S_1$	458.81	2.7023	1.2035	HOMO-2 (96) → LUMO (99)	4.8	0.937
					HOMO-1 (97) → LUMO (99)	12.2	
					HOMO (98) → LUMO (99)	31.4	
	$S_0 \rightarrow S_2$	402.55	3.0800	0.0155	HOMO-3 (95) → LUMO (99)	2.1	0.035
					HOMO-1 (97) → LUMO (99)	32.6	
					HOMO-1 (97) → LUMO+2 (101)	1.2	
					HOMO (98) → LUMO (99)	12.3	
	$S_0 \rightarrow S_3$	319.61	3.8793	0.0226	HOMO-4 (94) → LUMO (99)	2.4	0.051
					HOMO-2 (96) → LUMO (99)	40.0	
					HOMO (98) → LUMO (99)	2.6	
					HOMO (98) → LUMO+2 (101)	1.3	
M2	$S_0 \rightarrow S_1$	441.95	2.8054	1.1141	HOMO-2 (100) → LUMO (103)	5.4	0.923
					HOMO-1 (101) → LUMO (103)	14.3	
					HOMO (102) → LUMO (103)	28.8	
	$S_0 \rightarrow S_2$	386.01	3.2119	0.0127	HOMO-3 (99) → LUMO (103)	2.0	0.029
					HOMO-1 (101) → LUMO (103)	30.3	
					HOMO-1 (101) → LUMO+2 (105)	1.4	
					HOMO (102) → LUMO (103)	14.7	
	$S_0 \rightarrow S_3$	318.86	3.8884	0.1046	HOMO-5 (97) → LUMO (103)	2.8	0.214
					HOMO-4 (98) → LUMO (103)	2.3	
					HOMO-2 (100) → LUMO (103)	35.1	
					HOMO-1 (101) → LUMO (103)	1.4	
					HOMO (102) → LUMO (103)	2.2	
					HOMO (102) → LUMO+1 (104)	1.5	
					HOMO (102) → LUMO+2 (105)	1.3	

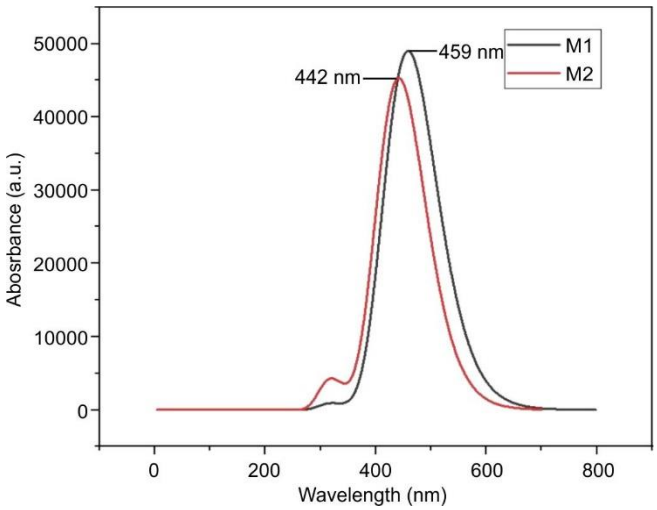

Fig. 4. Simulated UV-Vis absorption spectra of M1 and M2 calculated using CAM-B3LYP/6-31G(d,p)

analysis. The charge distribution across the donor, π-bridge and acceptor fragments was obtained by summing the atomic natural charges of the corresponding atoms. As listed in Table-4, the donor, π-bridge and acceptor charges were 0.719, -1.604 and 0.702 for M1, respectively, and 0.316, -0.216 and -0.100 for M2. The donor-acceptor charge difference Δq(D–A) calculated for M1 and M2 were found to be 0.017 and 0.416, respectively, which suggested that the internal polarization pattern is different for the two molecules.

TABLE-4
NBO CHARGE DISTRIBUTION OF DONOR, π-BRIDGE AND ACCEPTOR FRAGMENTS FOR THE PROPOSED CARBAZOLE DYES

Dyes	D	pi	A	$\Delta q_{(D-A)}$
M1	0.719	-1.604	0.702	0.017
M2	0.316	-0.216	-0.100	0.416

The charge distribution across the conjugated skeleton of M1 suggests higher delocalization than in M2, where the charge distribution is more localized between the donor and acceptor regions. Efficient intramolecular charge transfer (ICT) requires effective electron-density transfer from the donor to the anchoring acceptor. NBO analysis confirms the D-π-A character of both dyes, with M1 showing higher charge delocalization across the π-spacer than M2, which may facilitate photoinduced charge transfer. The MEP surfaces (Fig. 5) show a non-uniform electrostatic potential distribution across both molecules, consistent with their push–pull character [28,30,33]. M1 has minimum and maximum MEP values of -6.732×10^{-2} and $+6.732 \times 10^{-2}$, respectively, while the corresponding values for M2 are -6.697×10^{-2} and $+6.697 \times 10^{-2}$. The difference between the MEP extrema is small (3.5×10^{-4}), which indicate similar electrostatic characteristics for both dyes. This main difference occurs around the linker region, where the higher electronegativity of oxygen in M1 may result in a somewhat more negative electrostatic potential than the sulfur-containing linker of M2.

DOS, PDOS and TDM analysis: The DOS profiles further support the donor-π-acceptor electronic structure of both dyes (Fig. 6). The occupied frontier states mainly arise from the donor and π-bridge regions, whereas the unoccupied states are largely associated with the acceptor moiety. This spatial separation favours electron transfer following photoexcitation. The PDOS plots show clear fragment-wise contributions to the frontier states, with no pronounced mid-gap states. TDM analysis (Fig. 7) provides further information on electron–hole distribution and electronic coupling among the donor, π-spacer and acceptor units. The TDM maps show electronic interaction between these regions during excitation, consistent with the ICT characteristics obtained from the FMO and absorption analyses [8,33]. The DOS, PDOS and TDM results confirm suitable donor-to-acceptor electronic pathways in both dyes. M1 exhibits higher delocalization and stronger electronic coupling across the molecular framework, consistent with its comparatively favourable light-harvesting properties.

Reorganization energy: The reorganization energy provides a measure of the structural relaxation associated with charge transfer. As listed in Table-5, M1 has electron (λ_e), hole (λ_h) and total reorganization energies of 0.287, 0.155 and 0.442 eV, respectively, while M2 shows values of 0.268, 0.151 and 0.419 eV. For both dyes, λ_h is lower than λ_e, confirmed that lower structural relaxation for hole transport than for electron transport.

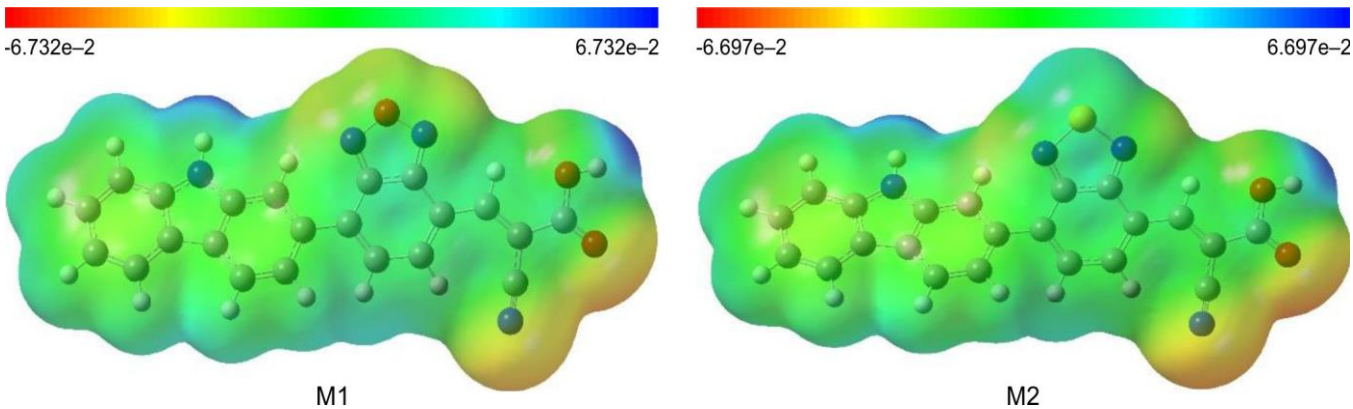

Fig. 5. Molecular electrostatic potential maps of M1 and M2

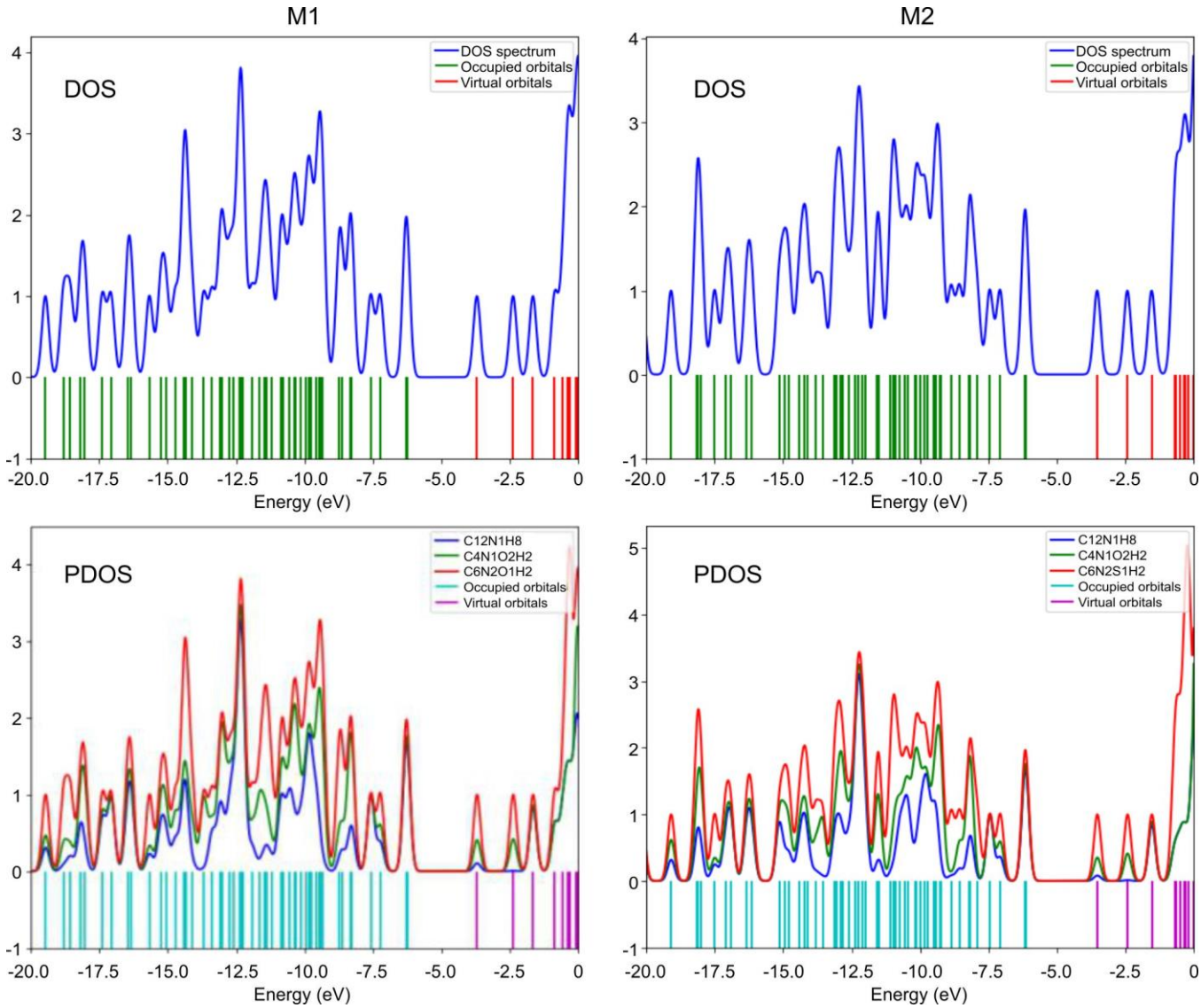

Fig. 6. Density of states (DOS) profiles and Partial density of states (PDOS) plots for M1 and M2 molecules

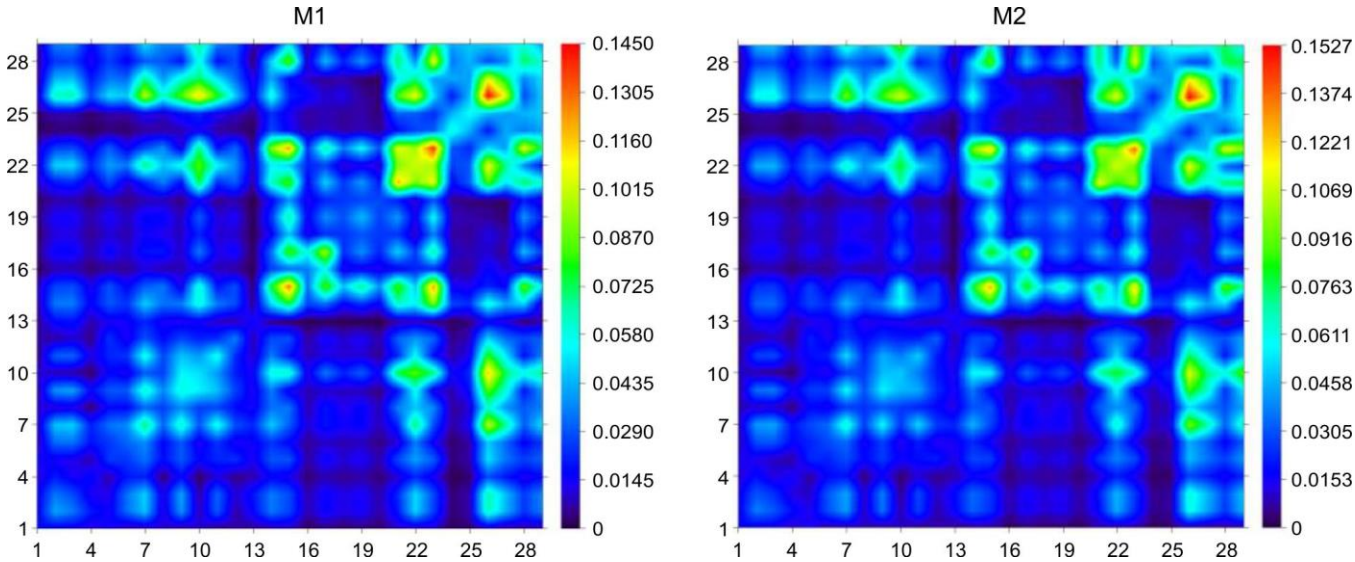

Fig. 7. Transition density matrix (TDM) maps of M1 and M2 molecules

TABLE-5
CALCULATED REORGANIZATION ENERGIES
OF THE TWO DESIGNED CARBAZOLE DYES

Molecule	λ_e (eV)	λ_h (eV)	λ_{total} (eV)
M1	0.287	0.155	0.442
M2	0.268	0.151	0.419

The reorganization energy was calculated using the following formula:

$$\lambda_{hole/electron} = [E^{\pm}(M) - E^{\pm}(M^{\pm})] + [E(M^{\pm})] - E(M)]$$

The term $E^{\pm}(M)$ is the energy of cation/anion with neutral geometry and $E^{\pm}(M^{\pm})$ represent the energy of cation/anion in their cationic/anionic geometries. Furthermore, $E(M^{\pm})$ is the energy of the neutral molecule at cationic/anionic state and E(M) correspond to the energy of the neutral molecule [36].

The slightly smaller total reorganization energy of M2 points to a reduced structural distortion in charge redistribution, which could be beneficial for charge-transport processes. The difference in total reorganization energy between the two molecules is approximately 0.023 eV, with M2 showing the lower value. Although the difference is not very large, its consistent direction for both electron and hole reorganization energies indicates that the O→S substitution does influence the structural relaxation associated with charge transfer. The suitability of a sensitizer for DSSC applications is governed by the combined effects of energy-level alignment, light absorption, excited-state charge transfer, electron injection, dye regeneration, charge transport and recombination, rather than by any single calculated parameter.

Considering the geometric, FMO and absorption results together, M1 appears more favourable than M2, with higher planarity, a smaller band gap, higher absorption intensity and higher LHE. The O→S substitution provides a means of tuning the balance between optical and electronic properties and charge-transport characteristics within the carbazole-based D-π-A framework. This structural variation provides insight into the relationship between molecular structure and the DSSC-relevant properties of carbazole-based sensitizers.

Photovoltaic parameter: The photovoltaic parameters were calculated to assess the suitability of the designed dyes as DSSC sensitizers. The power conversion efficiency (PCE), electron-injection free energy (ΔG_{inject}), dye-regeneration free energy (ΔG_{regen}), short-circuit current density (J_{sc}), fill factor (FF) and open-circuit voltage (V_{oc}) were considered to evaluate the charge-transfer and photovoltaic characteristics of the dyes. The HOMO energies of M1 and M2 were -6.056 and -5.991 eV, respectively, while the TiO_2 conduction-band edge was taken as -4.00 eV. The calculated electron-injection free energies were -4.758 eV for M1 and -4.796 eV for M2, which confirmed energetically favourable electron injection from the excited dyes into the TiO_2 conduction band. The regeneration driving forces were 1.206 eV for M1 and 1.141 eV for M2, supporting favourable regeneration through the electrolyte redox couple.

M2 showed a higher calculated V_{oc} (0.525 V) than M1 (0.356 V), while M1, exhibited higher oscillator strength (1.2035) and LHE (0.9374) than M2 (1.1141 and 0.9231, respectively). Using J_{sc} = 3.87 mA cm^{-2} and FF = 0.70 [34], the calculated PCE values were 0.965% for M1 and 1.424% for M2. Although M1 has more favourable optical properties, the higher V_{oc} calculated for M2 results in the higher estimated PCE. The equations used for calculating the photovoltaic parameters are given below.

The energy difference between the dye LUMO and the TiO_2 conduction-band edge was used to estimate the open-circuit voltage (V_{oc}). The V_{oc} (in eV) was calculated using the following relation:

$$V_{oc} = E_{CB} - E_{redox} \quad (1)$$

$$\Delta G_{inject} = E^{*}_{dye} - E_{CB} \quad (2)$$

The E^{*}_{dye} can be predicted from the following equation:

$$E^{*}_{dye} = E_{dye} - E_{\lambda max} \quad (3)$$

The following equation can calculate the dye regeneration free energy (ΔG_{regen}):

$$\Delta G_{regen} = E_{dye} - E_{electrolyte} \quad (4)$$

where $E_{electrolyte}$ redox is the electrolyte (I^{-}/I_3^{-}) redox potential and it is typically considered as (4.85 eV)

The power conversion efficiency (PCE, η) is a key parameter used to evaluate the efficiency of a DSSC in converting incident solar energy into electrical energy DSSC is a critical parameter that quantifies the effectiveness of the DSSC in converting solar energy into electricity. The formula for calculating η of a DSSC is

$$PCE = \eta = \frac{J_{mp}V_{mp}}{P_{inc}} = \frac{J_{sc}V_{oc}FF}{P_{inc}} = \frac{P_{max}}{P_{inc}} \quad (5)$$

where P_{inc} is the incident power from sunlight, representing the total amount of solar energy falling on the DSSC. The product of J_{sc}, V_{oc} and FF represents the maximum power output of the DSSC (P_{max}) under specific operating conditions.

The calculated photovoltaic parameters of M1 and M2 are listed in Table-6 along with representative carbazole-based DSSC dyes and established sensitizers for comparison. The calculated values for M1 and M2 fall within the range reported for related carbazole-based sensitizers.

Conclusion

In this study, two closely related carbazole-based D-π-A dyes, M1 and M2, were computationally investigated as potential sensitizers for dye-sensitized solar cells (DSSCs). The comparative analysis examined the effect of O→S substitution on their structural, optical, electronic and charge-transport properties. M1 exhibited a more planar structure, smaller HOMO–LUMO gap, red-shifted absorption, higher oscillator strength and higher light-harvesting efficiency than M2. Molecule M2 showed lower reorganization energy, higher calculated open-circuit voltage and higher calculated power conversion efficiency. Both dyes possessed favourable electron-injection and dye-regeneration driving forces. Under the adopted photovoltaic parameters, the calculated PCE values were 1.424% for M2 and 0.965% for M1. The results do not establish a clear overall advantage of either dye. Instead, the O→S substitution develops a distinct balance between optical, electronic and charge-transport properties. The study shows that heteroatom modification of the π-linker can be used to tune the properties of carbazole-based D-π-A sensitizers. These computational findings provide a basis for further molecular

TABLE-6
CALCULATED PHOTOVOLTAIC PARAMETERS OF THE TWO DESIGNED MOLECULES COMPARED WITH THE REPORTED CARBAZOLE-BASED SENSITIZERS

Molecules	f	LHE	ΔG_{inj} (eV)	ΔG_{reg} (eV)	V_{oc} (V)	FF	J_{sc} (mA cm^{-2})	PCE (eV)	Ref.
Thionothiophene (D1)	1.7187	0.981	-1.37	0.55	–	–	–	–	[29]
Diketopyrrolopyrrole (D2)	1.7079	0.980	-1.06	0.50	–	–	–	–	[29]
Bis(benzothiadiazole) (D3)	1.7437	0.982	-1.00	0.52	–	–	–	–	[29]
Bis(benzimidazole/benzimidazoline) (D4)	1.6041	0.975	-0.89	0.48	–	–	–	–	[29]
Thienopyridazine-type fused (D5)	1.6694	0.979	-0.91	0.34	–	–	–	–	[29]
Thienothiadiazole-type fused (D6)	1.7829	0.984	-0.90	0.32	–	–	–	–	[29]
Benzotriazole-type nitrogen-rich fused (D7)	1.3467	0.955	-0.60	0.28	–	–	–	–	[29]
Benzothiadiazole-type fused (D8)	1.3602	0.957	-0.56	0.38	–	–	–	–	[29]
CAR-THIOHX-1	–	–	–	–	0.722	0.69	3.19	1.58	[37]
CAR-THIOHX-2	–	–	–	–	0.646	0.64	3.93	1.62	[37]
CAR-THIOHX-3	–	–	–	–	0.736	0.74	3.36	1.83	[37]
CAR-TPA-1	–	–	–	–	0.720	0.70	3.87	1.94	[37]
CAR-TPA-2	–	–	–	–	0.610	0.68	4.19	1.75	[37]
CAR-TPA-3	–	–	–	–	0.755	0.76	3.72	2.12	[37]
Car-Cy	1.56	–	–	–	0.52	0.72	5.66	2.14	[38]
Car-Amin	1.78	–	–	–	0.54	0.71	5.95	2.27	[38]
Car-Mal	1.45	–	–	–	0.48	0.71	4.99	1.69	[38]
BG-501	0.025	–	–	–	0.560	0.60	7.46	2.49	[39]
BG-502	0.030	–	–	–	0.660	0.57	8.40	3.18	[39]
Z907	–	–	–	–	0.600	0.46	15.29	4.20	[39]
CVHTC	–	–	–	–	0.685	0.630	11.48	4.95	[40]
JY60	–	–	–	–	0.742	0.641	13.45	6.40	[40]
JY61	–	–	–	–	0.745	0.615	12.23	5.58	[40]
JY62	–	–	–	–	0.705	0.601	13.54	5.74	[40]
CVHTC	–	–	–	–	0.685	0.630	11.48	4.95	[40]
JY60	–	–	–	–	0.742	0.641	13.45	6.40	[40]
JY61	–	–	–	–	0.745	0.615	12.23	5.58	[40]
JY62	–	–	–	–	0.705	0.601	13.54	5.74	[40]
C1	–	–	-1.56	-0.38	0.040	0.27	1.63	0.016	[41]
C2	–	–	-1.21	-0.72	0.059	0.29	2.41	0.040	[41]
C3	–	–	-1.36	-0.64	0.017	0.17	1.00	0.001	[41]
P1 (reference)	–	–	–	–	0.045	0.26	4.06	0.047	[41]
Cz-2, I2-based electrolyte	–	–	–	–	0.648	0.68	8.02	3.51	[42]
Cz-2, I2-free electrolyte	–	–	–	–	0.685	0.54	8.50	3.13	[42]
M1	1.203	0.937	-4.758	1.205	0.356	0.700	3.870	0.964	Present work
M2	1.114	0.923	-4.796	1.141	0.525	0.700	3.870	1.423	Present work

design and optimization of DSSC dyes, while experimental studies are required to determine their actual photovoltaic performance.

CONFLICT OF INTEREST

The authors declare that there is no conflict of interests regarding the publication of this article.

DECLARATION OF AI-ASSISTED TECHNOLOGIES

During the preparation of this manuscript, the authors used an AI-assisted tool(s) to improve the language and no data, results or scientific conclusions were generated by AI. All analyses, interpretations and conclusions are the authors' own. The authors reviewed and edited the content and take full responsibility for the published work.

REFERENCES

1. G. Salerno, C.L. Boldrini, N. Manfredi, V. Capriati, O. Bettucci and A. Abbotto, *Commun. Chem.*, **9**, 70 (2026); https://doi.org/10.1038/s42004-025-01821-7
2. S.N. Tamilselvan and S. Shanmugan, *Clean Energy*, **8**, 238 (2024); https://doi.org/10.1093/ce/zkae031
3. R. Munir, A.F. Zahoor, M.N. Anjum, U. Nazeer, A.U. Haq, A. Mansha, A.R. Chaudhry and A. Irfan, *Top. Curr. Chem.*, **383**, 5 (2024); https://doi.org/10.1007/s41061-024-00488-3
4. K.S. Keremane, I.M. Abdellah, M.R. Eletmany, P. Naik, P. Anees and A.V. Adhikari, *J. Mater. Chem. C Mater. Opt. Electron. Devices*, **13**, 9258 (2025); https://doi.org/10.1039/D4TC04612A
5. I. Abubakari, *Comput. Theor. Chem.*, **1248**, 115165 (2025); https://doi.org/10.1016/j.comptc.2025.115165
6. K. Periyasamy, P. Sakthivel, G. Venkatesh, P. Vennila and Y.S. Mary, *Chem. Zvesti*, **78**, 447 (2024); https://doi.org/10.1007/s11696-023-03101-x
7. A. Arunkumar and P.M. Anbarasan, *J. Electron. Mater.*, **48**, 1522 (2019); https://doi.org/10.1007/s11664-018-06912-x

8. D. Slobodinyuk and A. Slobodinyuk, *Molecules*, **30**, 2423 (2025); https://doi.org/10.3390/molecules30112423
9. M. Eltoukhi, S.A. Badawy, A.A. Fadda, E. Abdel-Latif and M.R. Elmorsy, *J. Fluoresc.*, **35**, 9113 (2025); https://doi.org/10.1007/s10895-025-04194-1
10. A.D. Becke, *J. Chem. Phys.*, **98**, 5648 (1993); https://doi.org/10.1063/1.464913
11. C. Lee, W. Yang and R.G. Parr, *Phys. Rev. B Condens. Matter*, **37**, 785 (1988); https://doi.org/10.1103/PhysRevB.37.785
12. A.D. Becke, *J. Chem. Phys.*, **98**, 1372 (1993); https://doi.org/10.1063/1.464304
13. M.J. Frisch, G.W. Trucks, H.B. Schlegel, G.E. Scuseria, M.A. Robb, J.R. Cheeseman, G. Scalmani, V. Barone, G.A. Petersson, H. Nakatsuji, M. Caricato, A.V. Marenich, J. Bloino, B.G. Janesko, R. Gomperts, B.X. Li, Mennucci, H.P. Hratchian, J.V. Ortiz, A.F. Izmaylov, J.L. Sonnenberg, D. Williams-Young, F. Ding, F. Lipparini, F. Egidi, J. Goings, B. Peng, A. Petrone, T. Henderson, D. Ranasinghe, J. Gao, V.G. Zakrzewski, N. Rega, G. Zheng, W. Liang, M. Hada, M. Ehara, K. Toyota, R. Fukuda, J. Hasegawa, M. Ishida, T. Nakajima, Y. Honda, O. Kitao, H. Nakai, T. Vreven, K. Throssell, J.A. Montgomery Jr., J.E. Peralta, F. Ogliaro, M.J. Bearpark, J.J. Heyd, E.N. Brothers, K.N. Kudin, V.N. Staroverov, T.A. Keith, R. Kobayashi, J. Normand, K. Raghavachari, A.P. Rendell, J.C. Burant, S.S. Iyengar, J. Tomasi, M. Cossi, J.M. Millam, M. Klene, C. Adamo, R. Cammi, J.W. Ochterski, R.L. Martin, K. Morokuma, O. Farkas, J.B. Foresman and D.J. Fox, Gaussian 16, Revision B.01, Gaussian, Inc., Wallingford, CT (2016).
14. R. El Mouhi, A. Slimi, A. Fitri, A.T. Benjelloun, S. ElKhattabi, M. Benzakour, M. Mcharfi and M. Kurban, *Physica B*, **636**, 413850 (2022); https://doi.org/10.1016/j.physb.2022.413850
15. S. ElKhattabi, M. Hachi, A. Fitri, A.T. Benjelloun, M. Benzakour, M. Mcharfi and M. Bouachrine, *J. Mol. Model.*, **25**, 9 (2019); https://doi.org/10.1007/s00894-018-3888-0
16. H. Etabti, A. Fitri, A.T. Benjelloun, M. Hachi, M. Benzakour and M. Mcharfi, *Res. Chem. Intermed.*, **47**, 4257 (2021); https://doi.org/10.1007/s11164-021-04531-6
17. M. Hachi, A. Slimi, A. Fitri, A.T. Benjelloun, S. El khattabi, M. Benzakour, M. Mcharfi, M. Khenfouch, I. Zorkani and M. Bouachrine, *J. Photochem. Photobiol. Chem.*, **407**, 113048 (2021); https://doi.org/10.1016/j.jphotochem.2020.113048
18. M. Souilah, M. Hachi, A.T. Benjelloun, S. El Khattabi, M. Benzakour, A. Fitri, M. Mcharfi and H. Zgou, *Res. Chem. Intermed.*, **47**, 875 (2021); https://doi.org/10.1007/s11164-020-04302-9
19. O. Britel, A. Fitri, A.T. Benjelloun, M. Benzakour and M. Mcharfi, *J. Mol. Model.*, **28**, 351 (2022); https://doi.org/10.1007/s00894-022-05347-w
20. P. Naik, N. Swain, N. Devarajan, A.-B. Al-Odayni, N.A.Y. Abduh, R. Naik, K.S. Keremane, D. Alagarasan, T. Aravinda and H.B. Shivaprasad, *Heliyon*, **10**, e25624 (2024); https://doi.org/10.1016/j.heliyon.2024.e25624
21. S. Nadeem, M.U. Khan, R. Hussain, F. Shafiq and N. Alhokbany, *J. Chem. Technol. Biotechnol.*, **99**, 902 (2024); https://doi.org/10.1002/jctb.7595
22. Z. Shariatinia, *Nanoscale Adv. Mater.*, **2**, 137 (2025); https://doi.org/10.22034/nsam.2025.02.01
23. O. Britel, A. Fitri, A.T. Benjelloun, A. Slimi, M. Benzakour and M. Mcharfi, *J. Photochem. Photobiol. Chem.*, **428**, 113870 (2022); https://doi.org/10.1016/j.jphotochem.2022.113870
24. Z. Shariatinia, *J. Appl. Surf. Sci. Adv.*, **29**, 100846 (2025); https://doi.org/10.1016/j.apsadv.2025.100846
25. P. Verma and P. Chetti, *Chem. Phys. Impact*, **10**, 100789 (2025); https://doi.org/10.1016/j.chphi.2024.100789
26. E.A. Knyazeva, W. Wu, T.N. Chmovzh, N. Robertson, J.D. Woollins and O.A. Rakitin, *Sol. Energy*, **144**, 134 (2017); https://doi.org/10.1016/j.solener.2017.01.016
27. T. Lu and F. Chen, *J. Comput. Chem.*, **33**, 580 (2012); https://doi.org/10.1002/jcc.22885
28. M.S. Abusaif, M. Fathy, M. Abu-Saied, A.A. Elhenawy, A. Kashyout, M.R. Selim and Y.A. Ammar, *J. Mol. Struct.*, **1225**, 129297 (2021); https://doi.org/10.1016/j.molstruc.2020.129297
29. O. Britel, A. Fitri, A.T. Touimi Benjelloun, M. Benzakour and M. Mcharfi, *Chem. Phys.*, **565**, 111738 (2023); https://doi.org/10.1016/j.chemphys.2022.111738
30. T. Yakhanthip, S. Jungsuttiwong, S. Namuangruk, N. Kungwan, V. Promarak, T. Sudyoadsuk and P. Kochpradist, *J. Comput. Chem.*, **32**, 1568 (2011); https://doi.org/10.1002/jcc.21735
31. A. Ponnusamy Munusamy, A. Ammasi and M. Shkir, *Struct. Chem.*, **33**, 1097 (2022); https://doi.org/10.1007/s11224-021-01853-4
32. A. Ibrayeva, U. Abibulla, Z. Imanbekova, B. Baptayev, R.J. O'Reilly and M.P. Balanay, *Molecules*, **29**, 5035 (2024); https://doi.org/10.3390/molecules29215035
33. X. Liu, Z. Cao, H. Huang, X. Liu, Y. Tan, H. Chen, Y. Pei and S. Tan, *J. Power Sources*, **248**, 400 (2014); https://doi.org/10.1016/j.jpowsour.2013.09.106
34. Y.H. Cui, Y. Tong, L. Han, J. Gao and J.K. Feng, *J. Mol. Model.*, **25**, 249 (2019); https://doi.org/10.1007/s00894-019-4101-9
35. H. Etabti, A. Fitri, A.T. Benjelloun, M. Benzakour and M. Mcharfi, *Int. J. Comput. Theor. Chem.*, **12**, 2281050 (2024); https://doi.org/10.11648/j.ijctc.20241201.11
36. W. Zhang, L. Wang, L. Mao, J. Jiang, H. Ren, P. Heng, H. Ågren and J. Zhang, *J. Phys. Chem. C Nanomater. Interfaces*, **124**, 3980 (2020); https://doi.org/10.1021/acs.jpcc.9b10869
37. N. Duvva, R.K. Kanaparthi, J. Kandhadi, G. Marotta, P. Salvatori, F. De Angelis and L. Giribabu, *J. Chem. Sci.*, **127**, 383 (2015); https://doi.org/10.1007/s12039-015-0794-1
38. F. Ghasempour Nesheli, M. Tajbakhsh, B. Hosseinzadeh and R. Hosseinzadeh, *J. Photochem. Photobiol. Chem.*, **397**, 112521 (2020); https://doi.org/10.1016/j.jphotochem.2020.112521
39. C. Zafer, B. Gultekin, C. Ozsoy, C. Tozlu, B. Aydin and S. Icli, *Sol. Energy Mater. Sol. Cells*, **94**, 655 (2010); https://doi.org/10.1016/j.solmat.2009.11.014
40. Y.Q. Yan, Y.Z. Zhu, P.P. Dai, J. Han, M. Yan and J.Y. Zheng, *Sol. Energy*, **207**, 428 (2020); https://doi.org/10.1016/j.solener.2020.06.113
41. P. Naik, A. Planchat, Y. Pellegrin, F. Odobel and A.V. Adhikari, *Sol. Energy*, **157**, 1064 (2017); https://doi.org/10.1016/j.solener.2017.09.024
42. D.A. Chalkias, C. Charalampopoulos, S. Aivali, A.K. Andreopoulou, A. Karavioti and E. Stathatos, *Energies*, **14**, 1159 (2021); https://doi.org/10.3390/en14041159